2-Deoxy-D-glucose chemical exchange-sensitive spin-lock MRI of cerebral glucose metabolism after stroke in the rat

Running title: Metabolic MRI of stroke

Philipp Boehm-Sturm[1,2,3], Patrick Schuenke[4,5], Marco Foddis[1,2,3], Susanne Mueller[1,2,3], Stefan P. Koch[1,2,3], Daniel J. Beard[6], Paul Holloway[11,12], Amin Mottahedin[10,11,12], Leif Schröder[7,8,9], Alastair M. Buchan[1,11,12], Philipp Mergenthaler[1,3,11,12]

[1]Charité-Universitätsmedizin Berlin, Center for Stroke Research Berlin, Charitéplatz 1, 10117 Berlin, Germany

[2]Charité-Universitätsmedizin Berlin, corporate member of Freie Universität Berlin and Humboldt-Universität zu Berlin, Experimental Imaging at the Charité for 3R (EPIC3R), Charité 3[R] – Replace | Reduce | Refine, Berlin, Germany.

[3]Charité-Universitätsmedizin Berlin, Department of Neurology with Experimental Neurology, Berlin, Germany

[4]Charité-Universitätsmedizin Berlin, Department of Radiology, Berlin, Germany

[5]Physikalisch-Technische Bundesanstalt (PTB), Braunschweig and Berlin, Germany

[6]The University of Newcastle, School of Biomedical Sciences and Pharmacy, Australia

[7]German Cancer Research Center, Translational Molecular Imaging, Heidelberg, Germany

[8]Ruprecht Karls University Heidelberg, Department for Physics and Astronomy, Heidelberg, Germany

[9]German Cancer Consortium (DKTK), Heidelberg, Germany

[10]University of Oxford, Nuffield Department of Clinical Neurosciences, Oxford, United Kingdom

[11]University of Oxford, Radcliffe Department of Medicine, Oxford, United Kingdom

[12]Consortium International pour la Recherche Circadienne sur l'AVC (CIRCA)

Correspondence should be addressed to: Philipp Boehm-Sturm (philipp.boehm-sturm@charite.de) or Philipp Mergenthaler (philipp.mergenthaler@charite.de, Bluesky: @pm-lab.bsky.social)

Abstract

Rapid breakdown of cerebral glucose metabolism is a hallmark in stroke pathology. Metabolic activity delineates the penumbra from the infarct core, representing tissue that is potentially salvageable by therapeutic interventions. Tools to image dynamics of glucose and its spatial distribution could provide biomarkers of disease severity and of the success of therapeutic interventions.

Here, we developed a new protocol to measure glucose metabolism in a rat model of stroke using chemical exchange-sensitive spin-lock (CESL) MRI of the glucose analog 2-deoxy-D-glucose (2DG). We further implemented a protocol that combines 2DG-CESL-MRI with cerebral blood flow (CBF) and diffusion MRI. We found that 2DG-CESL-MRI provides a biomarker of disturbed glucose metabolism after stroke with high effect to noise ratios. This is the first study to investigate CESL MRI of 2DG in the context of metabolism imaging in rodent stroke.

Keywords: MRI, stroke, MCAO, CESL, Glucose Metabolism, 2-Deoxy-D-glucose

Introduction

The brain is almost exclusively relying on glucose as its main source of energy to sustain its function.[1, 2] In ischemic stroke, occlusion of a cerebral blood vessel leads to a rapid decline of oxygen, glucose and other metabolites in the affected brain region. Acute neurodegeneration is triggered by a range of mechanisms including apoptosis, mitochondrial dysfunction, and neuroinflammation.[3-7] Metabolic deficiency, and in particular glucose metabolism, is an important mechanism controlling acute neurodegeneration in stroke.[3, 8]

The ischemic penumbra is defined as the hypoperfused brain tissue around the necrotic infarct core.[3, 9, 10] The penumbra is characterized by decreased oxygen and glucose availability putting the cells of the neuro-glial-vascular unit in this tissue area at risk of death.[3] But if blood flow is restored, the penumbra is salvageable.[9, 10] The penumbra is highly dynamic, with diverse cellular and molecular mechanisms influencing tissue outcomes.[3] Clinical imaging of the penumbra typically focuses on blood flow and subsequent tissue damage.[11, 12] Despite the early adoption of metabolic imaging in understanding the penumbra[13-15], it remains largely inaccessible in both preclinical and clinical settings. Therefore, developing scalable methods to measure glucose metabolism is crucial for improving diagnostic tools and therapeutic stratification in stroke. Established methods include ex vivo autoradiography of ^{14}C-labeled glucose analogs such as 2-deoxy-d-glucose (2DG) and in vivo positron emission tomography (PET) of 18F 2-fluoro-2-desoxy glucose (18F-FDG)[16]. Both methods have their caveats, autoradiography is invasive and not applicable in longitudinal studies whereas 18F-FDG PET requires elaborate hardware and is heavily constrained by logistics such as proximity to a radiochemistry lab due to short half-life of the tracer and requires a dedicated radiation protection environment e.g. of nuclear medicine departments.

Magnetic resonance imaging (MRI) is broadly available and works with non-ionizing radiation. It has evolved as a key modality in stroke imaging since the contrast of MRI can be sensitized to different biological processes within one imaging session. For example, in ischemic stroke, dedicated sequences can measure reduced cerebral blood flow (CBF) and reduced apparent diffusion coefficient (ADC)[17] to assess acute hypoperfusion and the extent of the lesion core, respectively. The mismatch of these signals provides a noninvasive marker of the penumbra. Hyperintense signal in T2-weighted imaging provides a marker of vasogenic edema in subacute stroke and of necrotic tissue in older lesions[18]. These findings have triggered MRI-based diagnostic concepts in the context of preclinical and clinical research and successfully translated to acute stroke patient care in many specialized stroke units[18, 19].

Recently, MRI of natural D-glucose and glucose analogs has been achieved by utilizing chemical exchange between hydrogen bound to the molecule of interest and the larger water pool[20-25]. Chemical exchange sensitive spin lock (CESL) MRI is a particularly signal-to-noise ratio (SNR) efficient technique that measures the relaxation rate $R_{1\rho}$ in the rotating frame[26].

The goal of this study was to transfer these results to the context of stroke. We aimed to establish 2DG CESL MRI as a new biomarker of glucose metabolism in a rat model of ischemic stroke and combined it with T2-weighted, CBF and ADC imaging to relate this new biomarker with established MRI markers of tissue damage.

Material and Methods

Phantom experiments

Preliminary experiments with different 2DG solutions showed a dependency of R1ρ not only on 2DG concentration but also on pH and type of buffer. For the in vitro experiments shown in results, solutions of varying concentrations of 2DG in 1x Dulbecco's phosphate buffered saline (DPBS, Gibco, Thermo Fisher Scientific, Hennigsdorf, Germany) were prepared and filled in 5 mm NMR tubes (Carl Roth GmbH, Karlsruhe, Germany). The pH in the phantoms was measured at ~7.1.

Animals and study approval

Male Wistar rats (~8 weeks old, 280-320 g, n = 12) were used in this study. Rats were housed in a temperature, humidity and light (12/12-h light/dark cycle) environment. All animal procedures were performed after approval by the regulating authority (Landesamt für Gesundheit und Soziales Berlin). Studies were performed in accordance with the German Animal Welfare Act and EU regulations, and reporting follows the ARRIVE guidelines.

Anaesthesia and femoralis catheter

Animals were anesthetized using isoflurane in a 70%/30% N2O/O2 mixture. Anesthesia was induced with 5% isoflurane and maintained at 1.75-2.5% isoflurane during MCAO and 1.75% during MRI to achieve a breathing rate of ~60-100/min. A catheter (Portex Fine Bore Polythene Tubing, 0.58 mm inner diameter, 0.96 mm outer diameter, 90 cm long) was surgically placed and secured in the femoral vein for 2DG i.v. injections during MRI measurements.

Middle cerebral artery occlusion (MCAO) model of focal cerebral ischemia

Directly after placing the catheter, MCAO was surgically induced. A midline neck incision was made to expose the left common carotid artery and a ligature was tied around the common carotid artery (CCA) and the external carotid artery (ECA). After a small incision, a filament (390 µm diameter, 4039910PK10Re, Doccol, Sharon, MA/USA) was introduced into the CCA and advanced to the origin of the left MCA via the internal carotid artery. After 90 min, the filament was withdrawn. Both the CCA and ECA remained ligated during reperfusion. All MCAOs were performed by experienced surgeons.

MRI measurements

The experimental design is illustrated in Fig. 1. Directly after surgery, animals were transferred to a 7 T animal MRI (BioSpec 70/20 USR, Bruker, Ettlingen, Germany) using an 86 mm diameter volume coil for transmission, a rat surface coil for reception and Paravision 6.0.1 software. An MR compatible monitoring system (SA Instruments, Stony Brook, NY, USA) was used to continuously control animal temperature via a rectal probe and respiration rate via a pressure sensitive pad under the thorax. Animals were placed on an animal holder inside the MRI with ear and tooth bar fixation to avoid movement and in prone position. First, a localizer scan was acquired followed by B0 mapping and second order shimming (MAPSHIM). A simultaneous mapping of water shift and B1 (WASABI) sequence was used to check B0 and B1 homogeneity.[27] The protocol consisted of whole brain T2-weighted (T2w) MRI (2D RARE, 38 contiguous coronal slices with thickness 0.75 mm, field of view FOV = 33x33 mm^2, image matrix MTX = 220x220, repetition time TR = 4000 ms, RARE factor 8, echo spacing 11 ms, effective echo time TE = 33 ms, bandwidth BW = 34.7 kHz, number of averages NA = 3, total acquisition time TA = 5:25 min), 2DG CESL MRI (single 2.25 mm thick slice with FOV and geometry matching three slices of the T2w through the rostral-caudal center of the striatum), MTX = 110x110, TR = 5.4 ms, TE = 2.4 ms, BW = 46.9 kHz, 13 spin lock times (TSL) between 5-200 ms, adiabatic tipping using optimized HSExp pulses[28] and a matching spin lock pulse amplitude of B1 = 5 µT, NA = 1, 35 repetitions with TA = 1:26 min each, slow injection of 1 g/kg bodyweight 2DG i.v. after scan #5), diffusion MRI (SE-EPI, geometry matching the T2w, MTX = 128x128, TR = 3000 ms, TE = 20 ms, diffusion duration/separation = 2.5 ms/8.4 ms, 3 diffusion directions each with b = 650 s/mm^2 and b = 1300 s/mm^2, one b = 0 image, TA = 5:36 min), and arterial spin labeling MRI of CBF (FAIR-EPI, FOV = 33x33 mm^2, MTX = 128x96, single 1.0 mm thick slice with geometry matching the CESL MRI, 16 inversion times between 35 ms-1600 ms, recovery time 10 s, TE = 16 ms, BW = 357.1 kHz, TA = 5:45 min). Perfusion MRI was performed using global shimming (not local MAPSHIM) to ensure sufficiently homogeneous B0 profile outside the FOV to enable efficient global inversion pulses. For phantom experiments, the same CESL scan was used but with slice thickness of 2 mm, FOV = 16x16 mm^2 and MTX = 128x128.

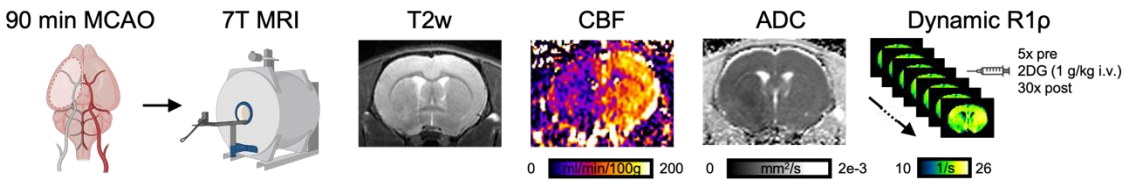

Fig. 1: Study design. Rats underwent 90 min transient MCAO. After surgery, animals were directly transferred to a 7 T MRI system for T2-weighted (T2w) MRI, perfusion MRI of cerebral blood flow (CBF), diffusion MRI of apparent diffusion coefficient (ADC) followed by dynamic R1ρ mapping with CESL MRI before and after injection of 2DG.

MRI data analysis

First, CESL images were motion-corrected in ANTx2 (https://github.com/ChariteExpMri/antx2)[29] using rigid (6 degrees of freedom) image registration of the later (i = 2…35) to the first CESL image dataset. For each time point, the first spin lock time image (TSL = 5 ms) was used for registration, the transformation was then applied to the other 12 TSL images.

$R_{1\rho}(t_i)$ maps at time t_i were calculated voxel-wise via mono-exponential fitting of CESL image signal intensities $S(t_i)$ over spin lock time TSL using the CESL signal equation:

$$S(TSL, t_i) = e^{-\mathrm{R1\rho}(t_i)\cdot \mathrm{TSL}};\ i = 1 \dots 35\ (1)$$

$\Delta R_{1\rho}(t_i)$ is a measure of local 2DG concentration and was calculated as the percent change with respect to the mean R1ρ during the first five baseline CESL scans:

$$\Delta \mathrm{R1\rho}(t_i) = \frac{\mathrm{R1\rho}(t_i) - \frac{1}{5}\sum_{i=1}^{5} \mathrm{R1\rho}(t_i)}{\frac{1}{5}\sum_{i=1}^{5} \mathrm{R1\rho}(t_i)} \times 100\%; i = 1 \dots 35\ (2)$$

Region-of-interest (ROI) analysis was performed in two ways (Fig. 2). In the first approach, brain regions were automatically segmented on the different MRI modalities (T2, ADC, CBF, CESL) using a series of 3D to 3D and 3D to 2D image registrations using the SIGMA rat brain template. The registration was then applied to the SIGMA atlas[30], which matches the template. For registration we used the b = 0 image for diffusion MR images, the first inversion time image for perfusion MR images and the first TSL image for CESL images. The transformation was then applied to the atlas to yield segmentations of the brain regions co-registered to ADC and CBF maps. For perfusion MRI, images were distorted due to shimming artefacts of the EPI sequence and a nonlinear registration was used. For ADC and CESL images, affine (12 degrees of freedom) registrations were sufficient.

For the second approach, the hypointense lesion was manually segmented on ADC, CBF and ΔR1ρ maps (mean image of the last 5 images) by an experienced researcher. Using the image registration transforms of the first approach, the lesion masks were transformed from ADC and CBF to the atlas and then registered to the ΔR1ρ maps. In atlas space, ROIs mirrored at the midline were automatically generated and also transformed to the ΔR1ρ maps. Lesion core was defined via hypointense ADC, hypoperfused tissue via hypointense CBF and the metabolic lesion was defined via hypointense areas on the mean ΔR1ρ maps (mean of the last 5 measurements). The penumbra was defined via perfusion diffusion mismatch, i.e.

$$mask_{penumbra} = mask_{hypoperfused} \setminus \left(mask_{hypoperfused} \bigcap mask_{core}\right)\ (3)$$

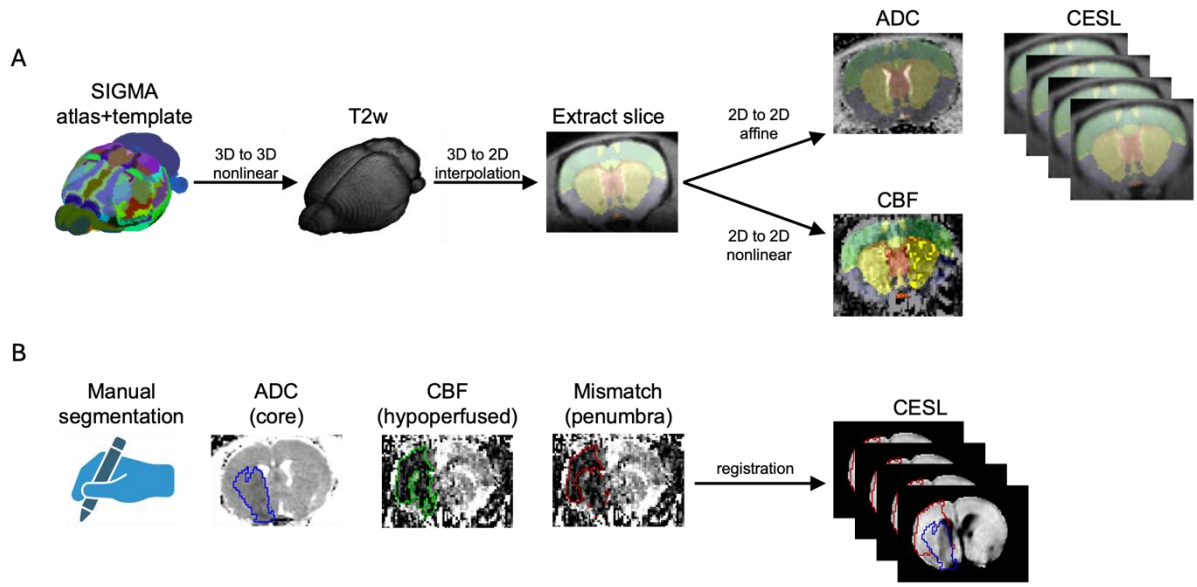

Fig. 2: ROI analyses. CESL images were quantified in anatomical regions defined in the SIGMA rat brain atlas (A) or using manual delineation of the lesion on ADC, CBF and late ΔR1ρ maps (mean of the last 5 maps). Penumbra was defined via perfusion/diffusion mismatch.

Statistics

Statistical analyses were performed in MATLAB (version 2021a, Natick, MA, USA). Values are expressed as mean ± 95% confidence interval (CI) for time courses and the correlation analyses. For the bar plots, mean ± standard deviation is shown. Effect sizes of ipsi- vs. contralateral mean values are reported as Cohen's d. Statistical analysis of ipsi- vs. contralateral values in the bar plots was performed using paired t-tests. Correlations of $\Delta R_{1\rho}$ with 2DG concentration and $\Delta R_{1\rho}$ with ADC and CBF were performed using Pearson correlation analyses. Lesion masks from the different modalities were compared using mask area and using Dice similarity coefficient with the metabolic lesion mask (derived from $\Delta R_{1\rho}$ maps) with all other masks. A test with $p < 0.05$ was considered statistically significant. Bonferroni correction of the significance level for multiple comparisons was used where indicated in the results.

Results

CESL MRI of phantoms containing different concentrations c_{2DG} of 2DG in buffer revealed the expected linear relationship with concentration (Fig. 3):

$$R1\rho = (8.35 \pm 0.30)\frac{1}{mM \cdot s} + (0.417 \pm 0.018);\ R^2 = 0.99\ (4)$$

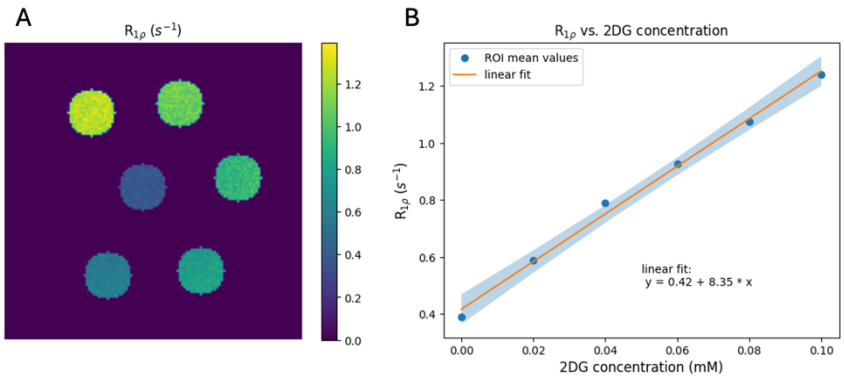

Fig. 3: Phantom experiments. R1ρ map of NMR tubes with different concentrations of 2DG (A) and linear fit of mean R1ρ within each tube over 2DG concentration (B).

In the rat MCAO model, we found a continuous increase of $R_{1\rho}$ over ~45 min in metabolically active contralateral tissue whereas $R_{1\rho}$ remained stable or even decreased in ipsilateral tissue (Fig. 4A, B). The decrease of R1ρ in the lesion can be explained by development of vasogenic edema and the accompanying decrease in transverse relaxation R2, which directly impacts R1ρ via R1ρ=Rex+R2. Rex summarizes relaxation in the rotating frame due to chemical exchange. When quantifying late $\Delta R_{1\rho}$ (mean of last 5 scans, Fig. 4C) the contrast was most pronounced in striatum (ipsi: -1.54±2.62%, contra: 2.80±1.45%, t = -5.27, p = 0.00026, significant after Bonferroni correction, Cohen's d = 1.52) and lesion core (ipsi: -1.11±2.70%, contra: 3.09±1.10%, t = -5.08, p = 0.00036, significant after Bonferroni correction, Cohen's d = 1.47) but smaller in hypoperfused tissue (ipsi: -1.04±2.76%, contra: 2.33±1.73%, t = -3.84, p = 0.0027, significant after Bonferroni correction, Cohen's d = 1.11) and not significant in the penumbra (ipsi: 0.04±3.19%, contra: 0.99±2.55%, t = -1.16, p = 0.27, Cohen's d=0.33).

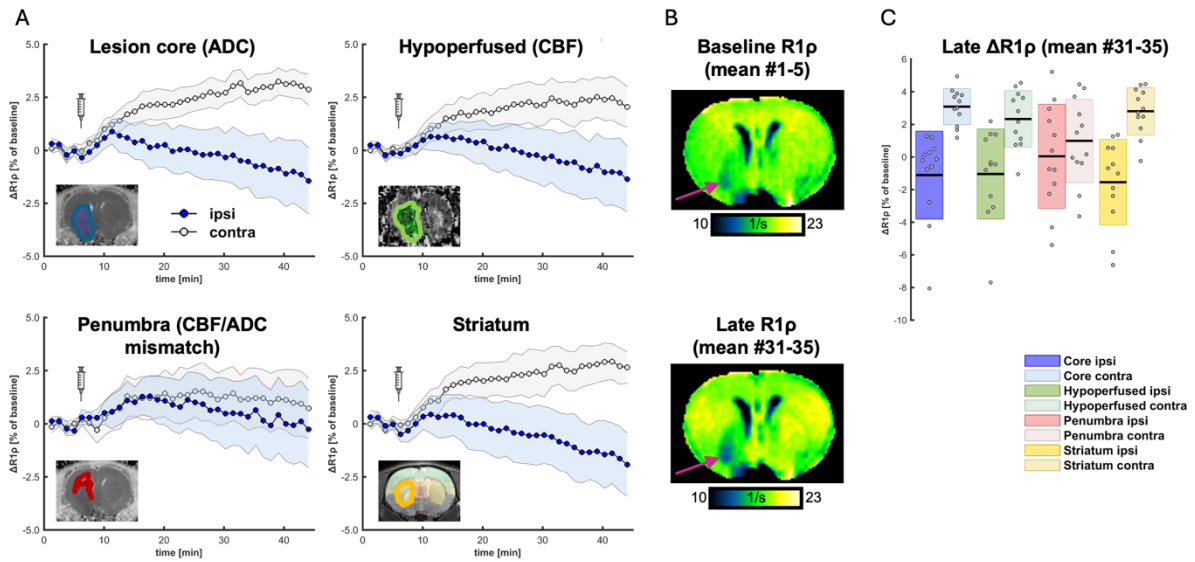

Fig. 4: In vivo metabolic MRI. Quantification of mean R1ρ in lesion core, hypoperfused area, penumbra, ipsilateral striatum (blue) and in corresponding mirrored ROIs (gray) showed strong differences that continuously increased over time. Shaded area corresponds to 95% CI (A). Representative baseline and late (mean of first and last 5 maps) R1ρ maps shows an increase in contralateral tissue and slight decrease in the lesion territory (B). Quantification of late R1ρ showed strongest effects of ipsi- vs. contralateral values in striatum and lesion core (C).

We then investigated how the new biomarker $\Delta R_{1\rho}$ (mean of last 5 scans) correlates with conventional MR biomarkers of focal cerebral ischemia, i.e. ADC (Fig. 5) and CBF (Fig. 6). A significant correlation was found only for ADC in the ipsilateral striatum (Pearson R = 0.65, p = 0.023).

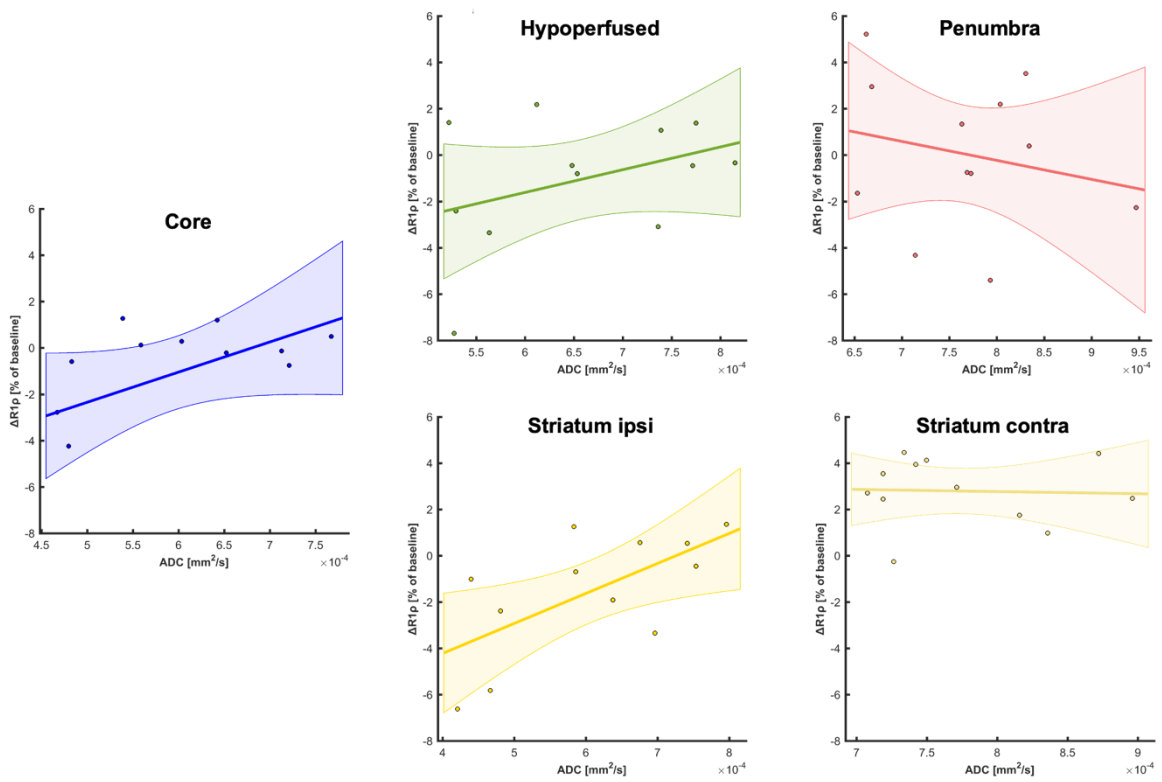

Fig. 5: Correlation of mean late ΔR1ρ with mean ADC in ROIs.

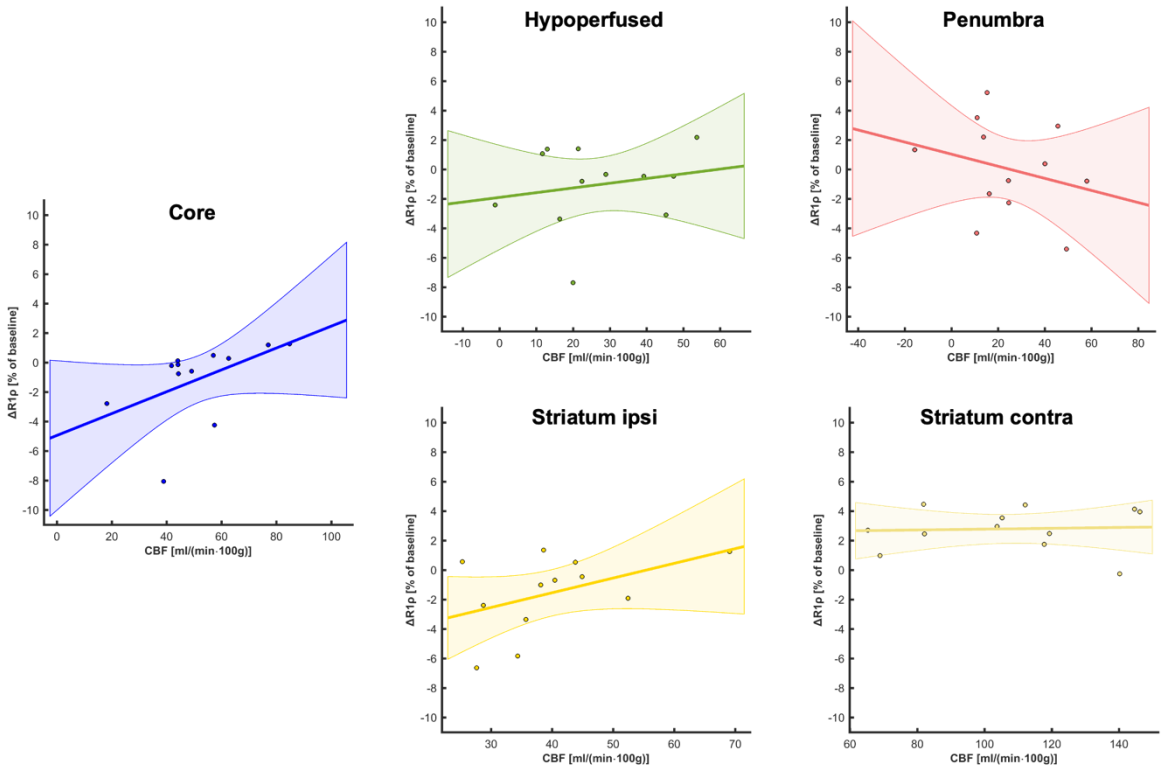

Fig. 6: Correlation of mean late ΔR1ρ with CBF in ROIs.

Finally, in a radiologist's approach, we wanted to investigate how the lesion mask derived from $\Delta R_{1\rho}$ maps, i.e. the metabolic lesion, correlates with the lesion defined via ADC and CBF maps. The metabolic lesion area (Fig. 7A) was smaller than lesion core ($A_{\Delta R1\rho}$= 14.63±8.79 mm^2 vs. A_{ADC} = 21.95±6.95 mm^2, t = -4.94, p = 0.0004, significant after Bonferroni correction) and hypoperfused area ($A_{\Delta R1\rho}$ vs. A_{CBF} = 26.48± 5.76 mm^2, t = -4.64, p = 0.0007, significant after Bonferroni correction) and comparable to penumbra ($A_{\Delta R1\rho}$ vs. $A_{penumbra}$= 10.86± 4.81 mm^2 t = 1.10, p = 0.30). Dice coefficient D similarity analysis (Fig. 7B) revealed most overlap with the lesion core ($D_{\Delta R1\rho,ADC}$ = 0.62±0.17), defined via ADC followed by hypoperfused area ($D_{\Delta R1\rho,CBF}$ = 0.50±0.16) and penumbra ($D_{\Delta R1\rho,penumbra}$ = 0.10±0.10). The pairwise differences between the three Dice coefficients were all significant after Bonferroni correction ($D_{\Delta R1\rho,ADC}$ vs. $D_{\Delta R1\rho,CBF}$, t = 5.34, p = 0.0002; $D_{\Delta R1\rho,ADC}$ vs. $D_{\Delta R1\rho,penumbra}$, t = 8.79, p = $3*10^{-6}$; $D_{\Delta R1\rho,CBF}$ vs. $D_{\Delta R1\rho,penumbra}$, t = 8.12, p = $6*10^{-6}$).

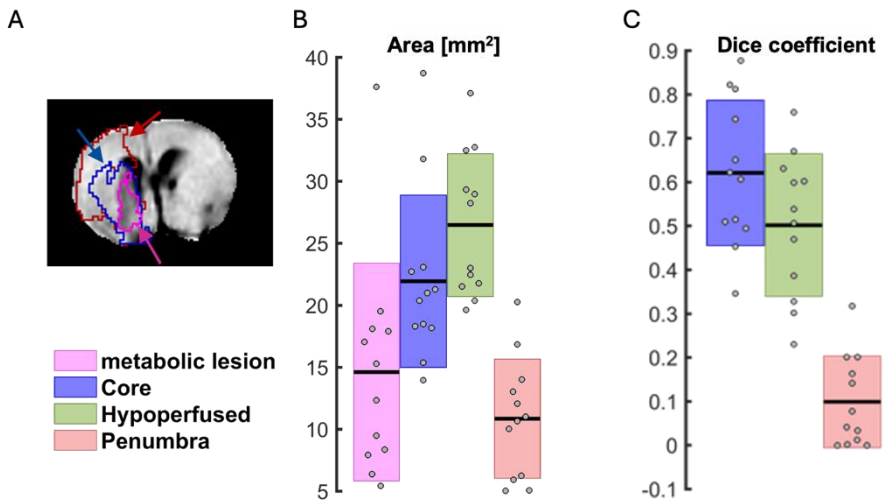

Fig. 7: Characterization of metabolic lesion mask defined via hypointense late ΔR1ρ. Delineated masks overlaid on ΔR1ρ map from representative animal (A). The metabolic lesion (magenta) is smaller than lesion core (blue) or hypoperfused area (green, B) and overlaps best with lesion core compared to hypoperfused area or penumbra (red) as assessed by Dice coefficient analysis (C).

Discussion

In this study, we established 2DG CESL MRI as a new biomarker for cerebral glucose metabolism in a rat model of ischemic stroke. We found that 2DG CESL MRI accurately delineated the ischemic core and allowed measuring cellular uptake of the glucose analogue in the penumbra. While 2DG CESL MRI provides conceptual information similar to 18F-FDG-PET imaging, the latter has not found wide adaptation due to the high costs and challenging logistics of producing radioisotopes, and the limited clinical availability of PET scanners for routine imaging. Furthermore, 2DG CESL MRI has superior spatial resolution compared to PET or deuterium metabolic imaging[31]. Furthermore, 2DG CESL MRI allows metabolic imaging with high effect sizes.

The size of the ischemic core in metabolic MRI was substantially smaller than resolved with conventional imaging biomarkers of stroke. While our study was not designed to address this, this raises the question whether the metabolic lesion represents the real ischemic core. A previous study investigating the utility in early MRI in predicting final infarct sizes in murine stroke demonstrated that the accuracy of ADC to predict the final infarct size depends on the time of imaging.[32] It is thus conceivable that the timing of imaging in our study was not optimal and that the metabolic infarct core is not representative of the final infarct size.

It should be noted that due to the high concentration of 2DG required for CESL MRI compared to FDG PET, it is presently not suitable as a translational tool. However, a previous study has used glucose for cerebral CESL imaging with reasonable signal-to-background[21], albeit different temporal kinetics, indicating that alternative carbohydrate tracers could provide a viable pathway for future clinical translation with further optimization. It was shown that after

injection of D-glucose or glucose analogs, $R_{1\rho}$ increased linearly with local concentration of the metabolite.[20, 21, 33] The authors concluded that 2DG CESL MRI can measure glucose transport and metabolism noninvasively in normal and pathological brain tissue. However, 2DG is trapped in cells and not further metabolized. 2DG CESL MRI is limited in that regard in the same way as 18F-FDG-PET. To this end, the recent introduction of dynamic nuclear polarization ("hyperpolarization") has made it possible to map the metabolism of carbon-13-labeled metabolic substrates in preclinical models[34, 35] and in humans[35-37] and achieves high spatial and temporal resolution as well as substantially improved signal-to-noise ratios.[35] Another recent study used deuterium (2H) metabolic imaging in combination with FDG-PET to study cerebral glucose metabolism after MCAO in mice.[31] While this approach allows for the mapping of glucose metabolites, it is at the expense of spatial resolution.[31]

As acute treatments like endovascular thrombectomy broaden therapeutic options for stroke, advanced imaging modalities play a crucial role in identifying patients who may benefit most from interventional therapy. The mismatch between perfusion and diffusion deficits is often considered a robust indicator of salvageable brain tissue,[38, 39] and mismatch imaging has become a crucial tool for stratifying patients and selecting therapies.[39, 40] To this end, integrating metabolic imaging, and precisely quantifying both the metabolic stroke core and metabolic penumbra at the time of emergency care, could further refine these treatment decisions. By providing essential data on tissue viability, metabolic imaging can improve our understanding of salvageable brain regions and inform on the potential reversibility of clinical deficits.

In summary, our present study demonstrates that 2DG CESL MRI provides new imaging biomarkers in preclinical stroke models which allows for multiplexing with other MR imaging modalities.

Acknowledgements

We thank Dr. Kai Herz for providing the adiabatic HSExp tipping pulses and Dr. Steffen Görke and Dr. Philip Boyd for helpful discussions during the planning of the study.

Author contributions

Concept and design: Boehm-Sturm, Mergenthaler

Acquisition, analysis, or interpretation of data: Boehm-Sturm, Schuenke, Foddis, Mueller, Koch, Mergenthaler

Discussion of the data: Boehm-Sturm, Schuenke, Foddis, Müller, Koch, Beard, Holloway, Mottahedin, Schröder, Buchan, Mergenthaler

Drafting of the manuscript: Boehm-Sturm, Mergenthaler

Critical review of the manuscript for important intellectual content: Boehm-Sturm, Schuenke, Foddis, Mueller, Koch, Beard, Holloway, Mottahedin, Schröder, Buchan, Mergenthaler

Statistical analysis: Boehm-Sturm, Schuenke, Koch

Supervision: Boehm-Sturm, Mergenthaler

Statements and declarations

Ethical considerations

Not applicable.

Consent to participate

Not applicable.

Consent for publication

Not applicable.

Declaration of conflicting interest

AMB is cofounder of BRAINOMIX. DJB is an inventor, and The University of Newcastle is applicant for the patent: *Stroke Treatment (WO 2022/072348)*. The other authors report no conflicts.

Funding statement

This work was funded by the Einstein Foundation Berlin (EJF-2020-602 to PM, EVF-2021-619 and EVF-2021-619-2 to PM and AMB) and the Leducq Foundation for Cardiovascular and Neurovascular Research (Leducq Foundation Trans-Atlantic Network of Excellence on Circadian Effects in Stroke, 21CVD04, PM and AMB). Funding to SM, MF, SPK and PBS was provided by the German Federal Ministry of Education and Research (BMBF) under the ERA-NET NEURON scheme (01EW2305), and the German Research Foundation (DFG, project BO 4484/2-1, Project-ID 424778381-TRR 295 ReTune and EXC-2049-390688087 NeuroCure). Noninvasive imaging experiments were supported by Charité 3R – Replace | Reduce | Refine. Funding to PS was profided by the Deutsche Forschungsgemeinschaft (DFG, Project-ID 372486779-SFB 1340 Matrix in Vision). DJB was supported by an EMBO Short-term Fellowship and funding from the National Health and Medical Research Council Australia (APP1182153). PM is Einstein Junior Fellow and AMB is Einstein Visiting Fellow, both funded by the Einstein Foundation Berlin. PM acknowledges funding from the Einstein Foundation Berlin (EJF-2020-602, EVF-2021-619, EVF-2021-619-2, EVF-BUA-2022-694), the Volkswagen Foundation (9A866), the Else Kröner-Fresenius Stiftung (2019-A34), and the Stiftung Charité (StC-VF-2024-59). Besides funding, the sponsoring organizations did not play any role in the preparation, review, or approval of the article, or decision to submit the article for publication.

Data and code availability

Data and code associated with this manuscript is available on Zenodo (https://zenodo.org/records/14526092; DOI: 10.5281/zenodo.14526091).

References

1. Mergenthaler P, Lindauer U, Dienel GA and Meisel A. Sugar for the brain: the role of glucose in physiological and pathological brain function. *Trends Neurosci* 2013; 36: 587-597.
2. Yellen G. Fueling thought: Management of glycolysis and oxidative phosphorylation in neuronal metabolism. *J Cell Biol* 2018; 217: 2235-2246.
3. Walther J, Kirsch EM, Hellwig L, et al. Reinventing the Penumbra - the Emerging Clockwork of a Multi-modal Mechanistic Paradigm. *Transl Stroke Res* 2023; 14: 643-666.
4. Niu X, Brahmbhatt H, Mergenthaler P, et al. A Small-Molecule Inhibitor of Bax and Bak Oligomerization Prevents Genotoxic Cell Death and Promotes Neuroprotection. *Cell Chem Biol* 2017; 24: 493-506 e495.
5. Endres M, Moro MA, Nolte CH, et al. Immune Pathways in Etiology, Acute Phase, and Chronic Sequelae of Ischemic Stroke. *Circ Res* 2022; 130: 1167-1186.
6. Chamorro A, Meisel A, Planas AM, et al. The immunology of acute stroke. *Nat Rev Neurol* 2012; 8: 401-410.
7. Moskowitz MA, Lo EH and Iadecola C. The science of stroke: mechanisms in search of treatments. *Neuron* 2010; 67: 181-198.
8. Mergenthaler P, Balami JS, Neuhaus AA, et al. Stroke in the Time of Circadian Medicine. *Circ Res* 2024; 134: 770-790.
9. Astrup J, Siesjo BK and Symon L. Thresholds in cerebral ischemia - the ischemic penumbra. *Stroke* 1981; 12: 723-725.
10. del Zoppo GJ, Sharp FR, Heiss WD and Albers GW. Heterogeneity in the penumbra. *J Cereb Blood Flow Metab* 2011; 31: 1836-1851.
11. Albers GW, Marks MP, Kemp S, et al. Thrombectomy for Stroke at 6 to 16 Hours with Selection by Perfusion Imaging. *N Engl J Med* 2018; 378: 708-718.
12. Nogueira RG, Jadhav AP, Haussen DC, et al. Thrombectomy 6 to 24 Hours after Stroke with a Mismatch between Deficit and Infarct. *N Engl J Med* 2018; 378: 11-21.
13. Heiss WD, Graf R, Wienhard K, et al. Dynamic penumbra demonstrated by sequential multitracer PET after middle cerebral artery occlusion in cats. *J Cereb Blood Flow Metab* 1994; 14: 892-902.
14. Heiss WD, Huber M, Fink GR, et al. Progressive derangement of periinfarct viable tissue in ischemic stroke. *J Cereb Blood Flow Metab* 1992; 12: 193-203.
15. Heiss WD and Zaro Weber O. Validation of MRI Determination of the Penumbra by PET Measurements in Ischemic Stroke. *J Nucl Med* 2017; 58: 187-193.
16. Sobesky J. Refining the mismatch concept in acute stroke: lessons learned from PET and MRI. *J Cereb Blood Flow Metab* 2012; 32: 1416-1425.

17. Schlaug G, Siewert B, Benfield A, et al. Time course of the apparent diffusion coefficient (ADC) abnormality in human stroke. *Neurology* 1997; 49: 113-119.
18. Sarraj A, Pujara DK and Campbell BC. Current State of Evidence for Neuroimaging Paradigms in Management of Acute Ischemic Stroke. *Ann Neurol* 2024; 95: 1017-1034.
19. Chen H, Lee JS, Michel P, et al. Endovascular Stroke Thrombectomy for Patients With Large Ischemic Core: A Review. *JAMA Neurol* 2024; 81: 1085-1093.
20. Jin T, Iordanova B, Hitchens TK, et al. Chemical exchange-sensitive spin-lock (CESL) MRI of glucose and analogs in brain tumors. *Magn Reson Med* 2018; 80: 488-495.
21. Jin T, Mehrens H, Hendrich KS and Kim SG. Mapping brain glucose uptake with chemical exchange-sensitive spin-lock magnetic resonance imaging. *J Cereb Blood Flow Metab* 2014; 34: 1402-1410.
22. Paech D, Schuenke P, Koehler C, et al. T1rho-weighted Dynamic Glucose-enhanced MR Imaging in the Human Brain. *Radiology* 2017; 285: 914-922.
23. Schuenke P, Koehler C, Korzowski A, et al. Adiabatically prepared spin-lock approach for T1rho-based dynamic glucose enhanced MRI at ultrahigh fields. *Magn Reson Med* 2017; 78: 215-225.
24. Schuenke P, Paech D, Koehler C, et al. Fast and Quantitative T1rho-weighted Dynamic Glucose Enhanced MRI. *Sci Rep* 2017; 7: 42093.
25. Xu X, Yadav NN, Knutsson L, et al. Dynamic Glucose-Enhanced (DGE) MRI: Translation to Human Scanning and First Results in Glioma Patients. *Tomography* 2015; 1: 105-114.
26. Jin T and Kim SG. Advantages of chemical exchange-sensitive spin-lock (CESL) over chemical exchange saturation transfer (CEST) for hydroxyl- and amine-water proton exchange studies. *NMR Biomed* 2014; 27: 1313-1324.
27. Schuenke P, Windschuh J, Roeloffs V, et al. Simultaneous mapping of water shift and B(1) (WASABI)-Application to field-Inhomogeneity correction of CEST MRI data. *Magn Reson Med* 2017; 77: 571-580.
28. Herz K, Lindig T, Deshmane A, et al. T1rho-based dynamic glucose-enhanced (DGErho) MRI at 3 T: method development and early clinical experience in the human brain. *Magn Reson Med* 2019; 82: 1832-1847.
29. Koch S, Mueller S, Foddis M, et al. Atlas registration for edema-corrected MRI lesion volume in mouse stroke models. *J Cereb Blood Flow Metab* 2019; 39: 313-323.
30. Barriere DA, Magalhaes R, Novais A, et al. The SIGMA rat brain templates and atlases for multimodal MRI data analysis and visualization. *Nat Commun* 2019; 10: 5699.
31. Meerwaldt AE, Straathof M, Oosterveld W, et al. In vivo imaging of cerebral glucose metabolism informs on subacute to chronic post-stroke tissue status - A pilot study combining PET and deuterium metabolic imaging. *J Cereb Blood Flow Metab* 2023; 43: 778-790.

32. Leithner C, Fuchtemeier M, Jorks D, et al. Infarct Volume Prediction by Early Magnetic Resonance Imaging in a Murine Stroke Model Depends on Ischemia Duration and Time of Imaging. *Stroke* 2015; 46: 3249-3259.
33. Jin T, Mehrens H, Wang P and Kim SG. Glucose metabolism-weighted imaging with chemical exchange-sensitive MRI of 2-deoxyglucose (2DG) in brain: Sensitivity and biological sources. *Neuroimage* 2016; 143: 82-90.
34. Grist JT, Bogh N, Hansen ES, et al. Developing a metabolic clearance rate framework as a translational analysis approach for hyperpolarized (13)C magnetic resonance imaging. *Sci Rep* 2023; 13: 1613.
35. Grist JT, Miller JJ, Zaccagna F, et al. Hyperpolarized (13)C MRI: A novel approach for probing cerebral metabolism in health and neurological disease. *J Cereb Blood Flow Metab* 2020; 40: 1137-1147.
36. Grist JT, McLean MA, Riemer F, et al. Quantifying normal human brain metabolism using hyperpolarized [1-(13)C]pyruvate and magnetic resonance imaging. *Neuroimage* 2019; 189: 171-179.
37. Lee CY, Soliman H, Geraghty BJ, et al. Lactate topography of the human brain using hyperpolarized (13)C-MRI. *Neuroimage* 2020; 204: 116202.
38. Demeestere J, Wouters A, Christensen S, et al. Review of Perfusion Imaging in Acute Ischemic Stroke: From Time to Tissue. *Stroke* 2020; 51: 1017-1024.
39. Simonsen CZ, Leslie-Mazwi TM and Thomalla G. Which Imaging Approach Should Be Used for Stroke of Unknown Time of Onset? *Stroke* 2021; 52: 373-380.
40. Thomalla G, Simonsen CZ, Boutitie F, et al. MRI-Guided Thrombolysis for Stroke with Unknown Time of Onset. *N Engl J Med* 2018; 379: 611-622.